CAMS Service Evolution

D1.1 Best estimate of dust emissions through offline inversion

Due date of deliverable	30/6/2025
Submission date	30/6/2025
File Name	CAMAERA-D1.1_v1.1
Work Package /Task	WP1
Organisation Responsible of Deliverable	BSC
Author name(s)	Jeronimo Escribano/Samuel Remy
Revision number	1.1
Status	
Dissemination Level	PU

Funded by the European Union

The CAMAERA project (grant agreement No 101134927) is funded by the European Union.

Views and opinions expressed are however those of the author(s) only and do not necessarily reflect those of the European Union or the Commission. Neither the European Union nor the granting authority can be held responsible for them.

1 Executive Summary

Dust emissions are a key component of atmospheric composition and air quality simulations. However, their representation are fraught with uncertainties arising from several factors: modelling issues arising from trying to parameterize the impact of very local processus such as saltation bombardment into global models with grid cells of several 10 of 100 of kilometres, errors in key meteorological variables such as wind speed and gusts, the impact of little known soil composition (silt, sand, clay) and soil characteristics (mean size of the soil particles). Besides, dust emissions are also very dependent on the modelling approach chosen, and in particular on the maximum particle size (20 micron radius in IFS-COMPO). This is why estimates of dust emissions vary so much in the literature.

Several dust emission datasets have been produced by inversion methods, such as in Escribano et al (2016, 2017) and the DUSTCOMM project (Adebiyi et al. 2020). However, none has been carried out with the IFS-COMPO atmospheric composition model. In this deliverable, an offline inversion of IFS dust emission has been performed using an ensemble approach. This methodology allowed us to derive best estimates of IFS-COMPO dust emissions, which minimize the error between simulated and observed dust optical depth. This dataset of corrected dust emissions is useful in order to diagnose systematic biases and issues in the operational dust emission scheme. This activity also provides a dataset of scaled emissions, which combines information from IFS-COMPO and observational data from the VIIRS sensor, which can be used to train machine learning methods. This dataset will be used for such a purpose in Work Package 6 of the CAMAERA project.

Table of Contents

2 Introduction

2.1 Background

The European Union's flagship Space programme Copernicus provides a key service to the European society, turning investments in space-infrastructure into high-quality information products. The Copernicus Atmosphere Monitoring Service (CAMS, https://atmosphere.copernicus.eu) exploits the information content of Earth-Observation data to monitor the composition of the atmosphere. By combining satellite observations with numerical modelling by means of data assimilation and inversion techniques, CAMS provides a wealth of near-real time information to answer questions related to air quality, climate change and air pollution and its mitigation, energy, agriculture, etc. CAMS provides both global atmospheric composition products, using the Integrated Forecasting System (IFS) of ECMWF - hereafter denoted as the *global production system* -, and regional European products, provided by an ensemble of eleven regional models - the *regional production system*.

The CAMS AERosol Advancement (CAMAERA) project will provide strong improvements of the aerosol modelling capabilities of the regional and global systems, on the assimilation of new sources of data, and on a better representation of secondary aerosols and their precursor gases. In this way CAMAERA will enhance the quality of key products of the CAMS service and therefore help CAMS to better respond to user needs such as air pollutant monitoring, along with the fulfilment of sustainable development goals. To achieve this purpose CAMAERA will develop new prototype service elements of CAMS, beyond the current state-of-art. It will do so in very close collaboration with the CAMS service providers, as well as other tier-3 projects. In particular CAMAERA will complement research topics addressed in CAMEO, which focuses on the preparation for novel satellite data, improvements of the data assimilation and inversion capabilities of the CAMS production system, and the provision of uncertainty information of CAMS products.

2.2 Scope of this deliverable

2.2.1 Objectives of this deliverable

This deliverable documents the production of the dataset of dust emission inversions associated with Task 1.1 of CAMAERA. Dust emission inversions were computed by the ingestion of dust-filtered satellite observations of aerosol optical depth (AOD) in a modified version of the Local Ensemble Transform Kalman Filter, where the model ensemble was constructed with a series of IFS-COMPO simulations. The resulting emissions have been tested in the forecast model (IFS-COMPO) and the simulated AOD has been evaluated against ground-based measurements. This deliverable presents the inversion method and their outcome verification by *posteriori* simulations.

2.2.2 Work performed in this deliverable

In this deliverable the work as planned in the Description of Action (DoA, WP1 T1.1) was performed.

2.2.3 Deviations and counter measures

No deviations have been encountered.

2.2.4 CAMAERA Project Partners:

HYGEOS	HYGEOS SARL
ECMWF	EUROPEAN CENTRE FOR MEDIUM-RANGE WEATHER FORECASTS
Met Norway	METEOROLOGISK INSTITUTT
RC.io	RESEARCHCONCEPTS IO
BSC	BARCELONA SUPERCOMPUTING CENTER-CENTRO NACIONAL DE SUPERCOMPUTACION
KNMI	KONINKLIJK NEDERLANDS METEOROLOGISCH INSTITUUT-KNMI
SMHI	SVERIGES METEOROLOGISKA OCH HYDROLOGISKA INSTITUT
FMI	ILMATIETEEN LAITOS
MF	METEO-FRANCE
TNO	NEDERLANDSE ORGANISATIE VOOR TOEGEPAST NATUURWETENSCHAPPELIJK ONDERZOEK TNO
INERIS	INSTITUT NATIONAL DE L ENVIRONNEMENT INDUSTRIEL ET DES RISQUES - INERIS
IOS-PIB	INSTYTUT OCHRONY SRODOWISKA - PANSTWOWY INSTYTUT BADAWCZY
FZJ	FORSCHUNGSZENTRUM JULICH GMBH
AU	AARHUS UNIVERSITET
ENEA	AGENZIA NAZIONALE PER LE NUOVE TECNOLOGIE, L'ENERGIA E LO SVILUPPO ECONOMICO SOSTENIBILE

3 Methodology: LETKF applied to IFS-COMPO dust ensemble simulations

3.1 Overview

We used the core of the Local Ensemble Transform Kalman Filter (LETKF, Hunt et al 2007) algorithm to compute the best estimates of *a posteriori* emissions, given an ensemble of forward model simulations and dust-filtered satellite observations. The proposed methodology allows offline assimilation experiments by choosing a distinct approach for the temporal and the spatial attribution of the increments. The control variable of the system is the dust emission, which has the spatial resolution of the forward numerical model. Corrections to the prior emissions are computed for contiguous periods of 3 days for all the simulation. Detail on the method are shown in Section 3.3 and Figure 2. Posterior observables, like the aerosol optical depth, are computed by running a single (deterministic) model simulation that uses the posteriori emission corrections computed by the data assimilation (DA) system.

The verification of the results and the changes induced by the assimilation is done by comparing aerosol optical depth measured by AERONET in sites with predominance of dust. We provide a qualitative overview of the dust emission analyses increments and the verification with AOD observations.

3.2 Observations

We assimilate AOD observations from Suomi-NPP VIIRS Deep Blue version 1. Level 2 550nm AOD were filtered by the Quality Assurance flag equal 3 over Ocean and 2 over land. We only use those retrievals flagged as “dust”. The ~ 6 km retrievals were averaged and projected to the regular 0.5 degrees latitude-longitude grid of the post processed IFS-COMPO outputs. A minimum threshold on the numbers of retrieval was imposed in order to avoid large sampling errors, retaining AOD retrievals that cover around 20% or more of the model grid cell area. The observational error has been set to the same values as in Escribano et al. (2022), that is, 0.2xAOD + 0.05.

The observation operator in the system is the full IFS-COMPO, as it outputs time-dependent AOD fields based on input emissions. We have produced two experiments that differ on the observation operator (see Section 3.4 for the justification of the two experiments). The first experiment uses the *dust* AOD (DOD) from IFS-COMPO, while the second uses the *total* AOD from IFS-COMPO.

3.3 Ensemble strategy

In this ensemble data assimilation approach, the ability of controlling the variables is largely determined by the design of the ensemble. The perturbations of the emissions (the control variable) are propagated to the AOD (the observable) by the model. Therefore, the ensemble itself determines the subspace where the analysis can be explored for the control variables. In this case, the ensemble is constructed by perturbing emissions in both time and space, to allow the effective control of the emission variables in these dimensions.

For the spatial dimension we have followed the emission perturbation approach from Escribano et al. (2022) by using correlated gaussian noise multiplying the IFS-COMPO dust emissions. The maps have correlation lengths of 250 km globally, as shown in Figure 1. The correlation length of 250 km was set to roughly be comparable to the size of dust emission hotspots and regions; meaning that the inversion system should be able to correct emissions in this spatial scale. We will show in the final sections how this correlation length is being revised.

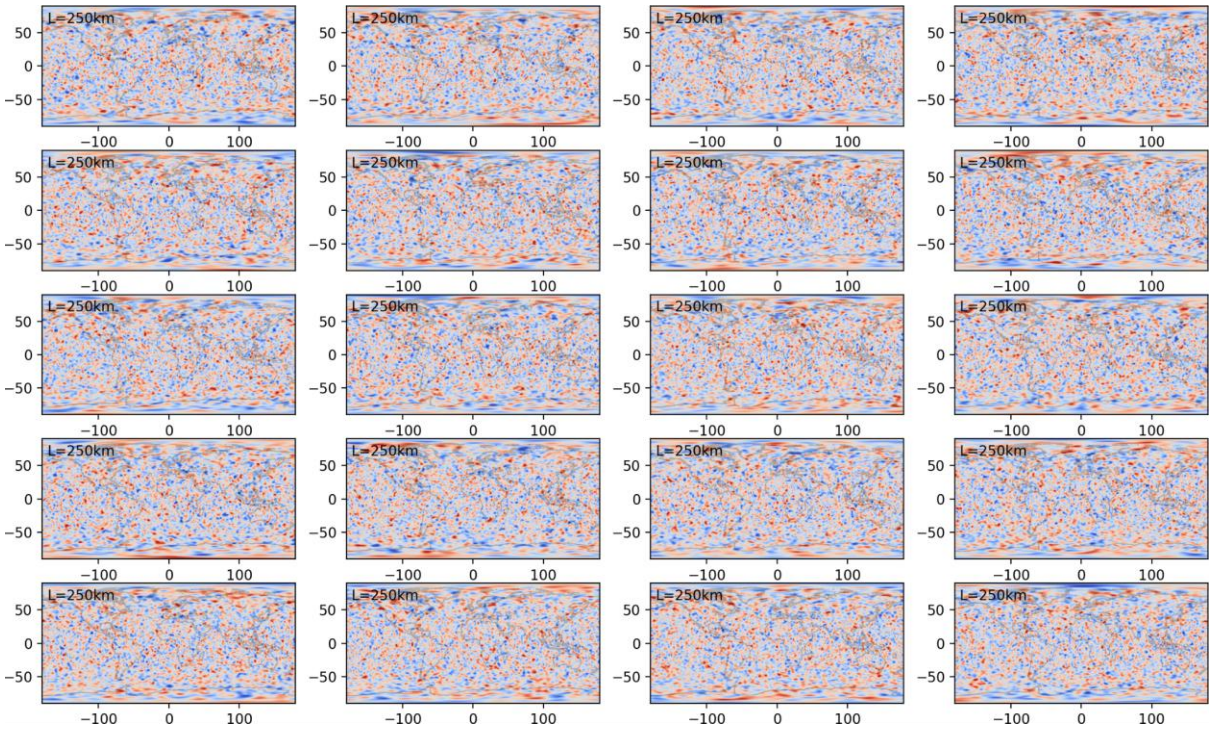

Figure 1: Random gaussian perturbation maps with length scale of 250 km used in the ensemble generation.

For the temporal dimension (c.f. Figure 2), the design of the ensemble aims that the departures between model and observations can be correctly attributed to increments in emissions at the proper space and time of emission. This implies that the control vector must be defined with the temporal dimension in it, and so the ensemble produced accordingly. Because the residence time of tropospheric aerosols is in the order of days, it is not expected that changes in aerosol emissions can have noticeable influence on the satellite observable AOD after around 10 to 15 days of being emitted. In the same manner, the spatial influence of dust aerosol emissions is on the order of a few thousand kilometres for this rough estimate of its residence time. That said, a clear path of accounting for the temporal attribution of the increments is by differentiating aerosol emissions from different days in the ensemble. This can be done easily in two ways (without tangent linear or adjoint computations): (i) A first idea would be to use a tagging technique to identify the time (back in hours or days) that the airborne aerosol has been emitted in the model. This approach requires in practice technical developments in the model regarding I/O and memory usage that are quite cumbersome; (ii) A second option, which is implemented in this system, is to tag the timing of the aerosol emission by simply creating different ensembles, or, which is equivalently in a linear system, creating a time finite difference method to estimate the sensitivity of the AOD to the emissions. Therefore, in this approach the emissions are perturbed for a defined period of time (let's say, from day 0 to day D) and then the model keeps running with the unperturbed emissions for the rest of the simulation, or until the influence of the emissions perturbations can be considered negligible in the system. As argued before, we set this window to 15 days. In this approach if we aim for daily resolution of the control (D=1), we should produce a 15-days ensemble forecast. The final configuration of the ensemble uses D=3, meaning that the final emissions corrections will be produced with a time resolution of 3 days, which uses, at the end, 5 times more HPC hours than a single ensemble simulation, but 3 times less than a daily resolution control vector ensemble.

The diagram of Figure 2 shows the rationale of the temporal perturbations of dust emissions used in the construction of the IFS-COMPO ensemble. In practice, same-colour members can

be compressed in the same IFS experiment because they share the same perturbation strategy (and map) and they do not overlap in time.

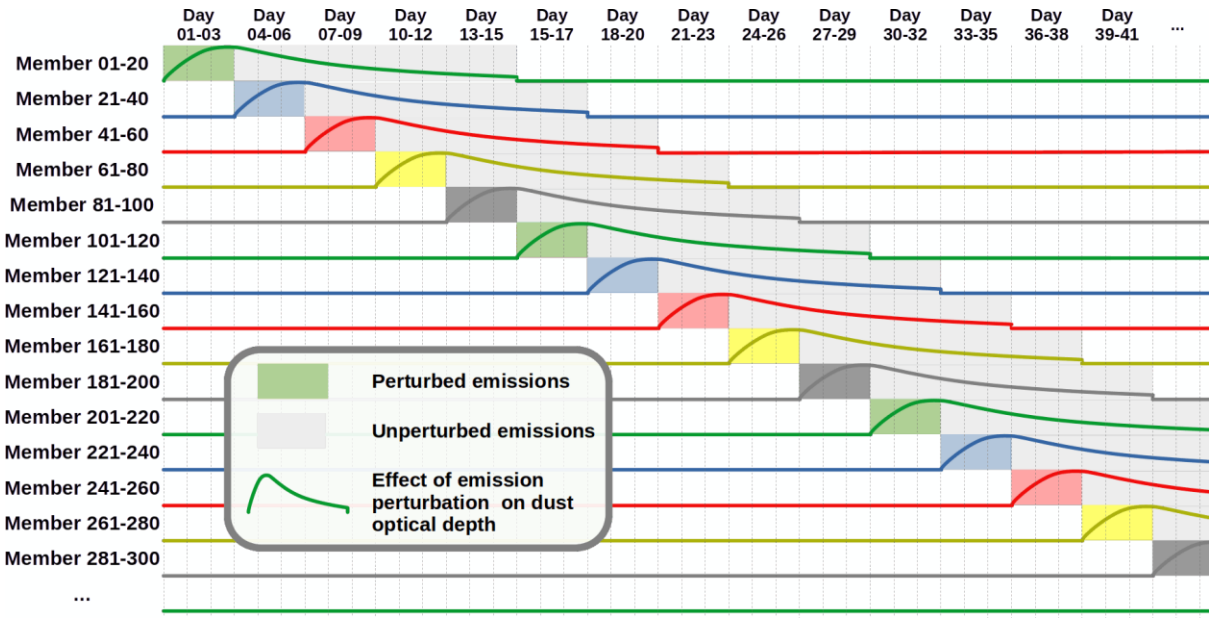

Figure 2: Ensemble generation strategy. Coloured boxes indicate dates when the emissions are perturbed. Gray-shaded boxes indicate when the simulation runs with unperturbed emissions. Colour lines aim to represent the effect of the emission perturbation in the AOD.

3.4 Evaluation of the prior simulations

The IFS-COMPO ensemble of dust emissions used in the LETKF has the following characteristics:

- 1 control and 20 perturbed members,
- 15 days forecasts, cycling every three days, no data assimilation,
- Meteorology nudged to ERA-5 during the forecast,
- Perturbation of dust emissions applied in the first three days,
- TL511 L137 resolution (~39 km horizontal resolution, 139 vertical levels),
- Aerosol only IFS-COMPO pre cycle 50R1 version, no chemistry configuration,
- Processed from 31/12/2016 to 1/1/2022 (5 years).

The control run has been evaluated against AERONET observations of aerosol optical depth (AOD) at 500 and 1020 nm (see Figure 3) over a selection of 23 stations representative of desert dust conditions (Figure A1). The comparison shows that the control run manages to simulate well the variations of observed AOD at 500 and 1020nm. The mean Pearson correlation factor between the observed and simulated AOD datasets stands at 0.82 over the 5-year period for AOD at 500nm, and 0.8 for AOD at 1020nm.

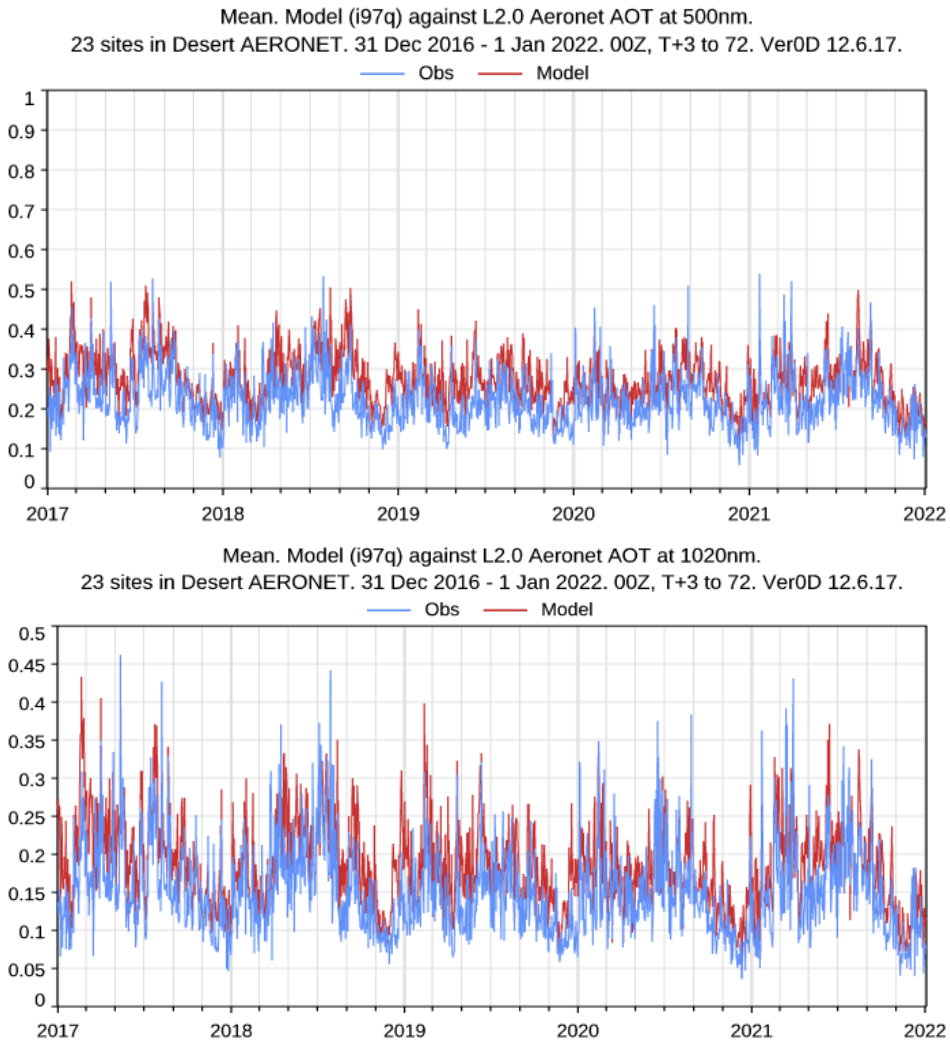

Figure 3: Comparison of daily simulated (red) and observed AOD at 500nm (top) and 1020nm (bottom) from 31/12/2016 to 1/1/2022. Observations are from level 2 AERONET over a selection of 23 desert dust impacted stations (see Section A1).

Control IFS-COMPO produced two simulated optical depth quantities, AOD and *Dust Optical Depth* (DOD). When comparing the IFS simulations with VIIRS dust-filtered AOD (which are the assimilated observations), the simulated AOD fields of IFS shows better skills than the simulated DOD fields. Fig. 4 shows this mismatch for IFS DOD (left) and IFS AOD (right), in comparison with VIIRS dust-filtered AOD (top) and AERONET AOD (filtered by Ångström exponent < 0.3, middle) and 23 selected AERONET stations (bottom). We found an underestimation of the control simulation DOD with respect to the assimilated observations and to the AERONET dust–filtered AOD (Ångström<0.3). Therefore, before assimilation, a bias correction is applied to the model DOD using a multiplicative scaling factor of 1.5 to the model simulated DOD, hereinafter denoted by DUODx1.5_SCALING. For AOD, the use of the outputs of the model in the assimilation experiment remains unaltered and it is denoted by AOD_SCALING experiment. Possible causes for the underestimation of IFS DOD with respect to VIIRS or AERONET AOD can be (i) due to an underestimation of dust in the model, or (ii) because the comparison is made between DOD and observational AOD, although filtered by dust scenes it still can contains a non-dust contribution.

	IFS-COMPO DOD	IFS-COMPO AOD
VIIRS dust-filtered AOD	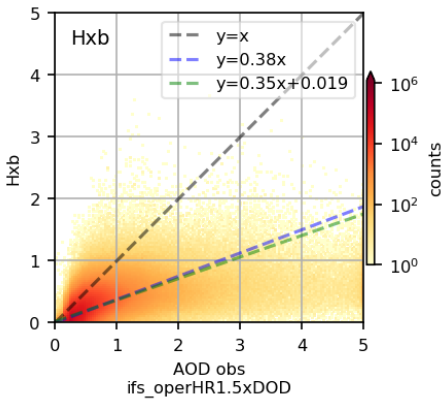	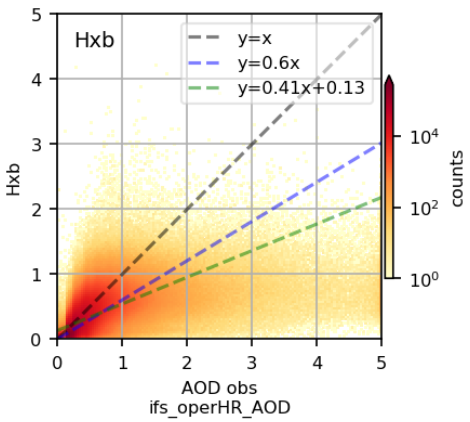
AERONET (Ångström <0.3, all stations)	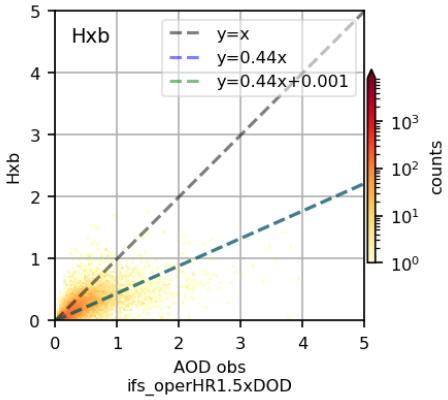	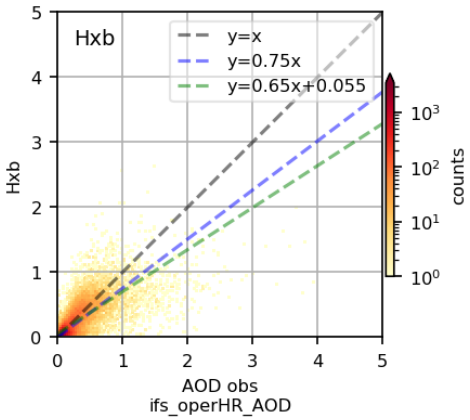
AERONET (all points, 23 selected stations)	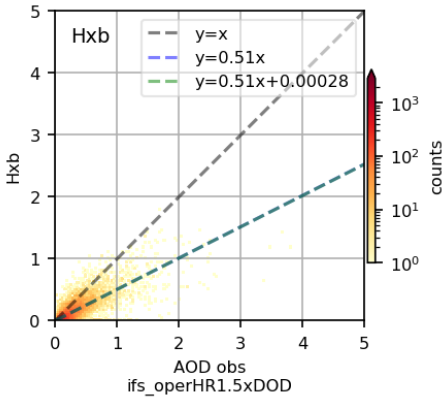	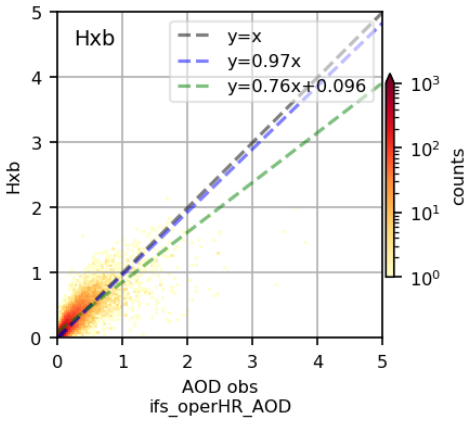

Figure 4: Histograms of collocated (3-hourly) comparison between IFS-COMPO dust AOD (left), total AOD (right) with dust-filtered AOD (top), Ångström-filtered AERONET 550nm (middle) and AERONET AOD from 23 selected stations dominated by dust (bottom). Observations are on the x-axis and model simulations on the y-axis. Fitted linear regression lines are drawn in green, and fitted regression without intercept is drawn in blue.

Figure 5 shows the impact of the dust emission perturbations on the simulated global dust emissions and burden in 2017, as compared to the control run which doesn't apply perturbations, after 72h of forecast using perturbed dust emissions. The envelope of the minimum-maximum values of the perturbed emissions represents generally between 10 and

20% of the total dust emissions. For the simulated burden, the impact of the perturbation is roughly of the same range, 10-20% of the control run burden.

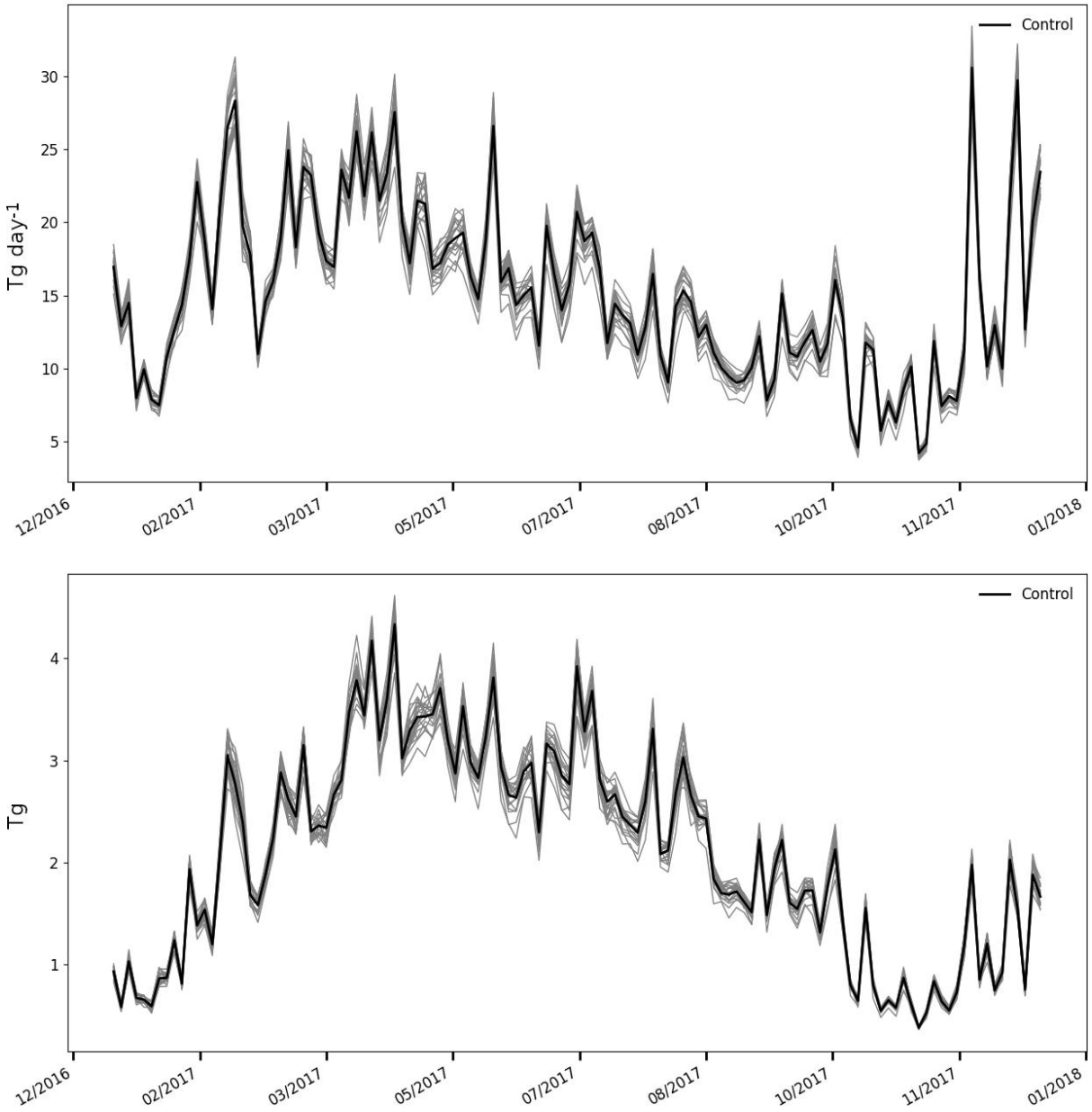

Figure 5: Simulated global dust emissions (top) and tropospheric mass (bottom) by the IFS-COMPO ensemble at 72h forecast time. The control is shown in bold black line; the 20 perturbed members are shown in grey. Only members with active emission perturbations are included in this figure (i.e., those with filled colours in Figure 2).

3.5 Data assimilation and covariance inflation

The data assimilation is performed by using the ensemble in a LETKF system. The parallelization strategy proposed with this method (as in Hunt et al., 2007) uses the domain decomposition to efficiently compute the analysis in an HPC environment. In this work, we extend the idea of the spatial domain decomposition to the time dimension. Both decompositions rely on a reasonable value of the localization parameter, which in the LETKF

algorithm is done in the observational space. Because dust emissions (and their perturbation footprint) can travel thousands of kilometres for several days, we use a gaussian localization with spatial length scale of 2000 km, and the temporal length scale of 12 days. This provides an optimal use of the observation and takes advantage of the current ensemble design. Given these parameters, the analysis is computed independently for each day and uses observations up to around 1.5 months away from that day, within a radius of 2000 km. The large assimilation window is because the LETKF estimates the emissions for the whole window, and emissions of days near in time can modify the analyses of the target day (because they can mix and overlap during transport), or in other words, the assimilation window should be long enough to ensure a continuous transition between the chunks computed independently. This is the same approach used in the LETKF of Hunt et al. (2007) for the spatial decomposition.

The temporal decomposition of the ensemble in finite-difference approach, as shown in Figure 2, produces a large decrease of the ensemble covariance of emissions and of AOD with respect to a standard construction of the ensembles. As an example, for a given day (e.g. day 22 of Figure 2, with the box coloured red), the assimilation window will be between day 8 to day 37 (previous and following box coloured red). This implies a size of the ensemble for the computation of the analysis of this day of 10 blocks x 20 members each = 200 members, from where only 20 of them (the ones of day 21-23) have perturbed emissions, and 100 of them have perturbed AOD (i.e., those that had perturbed emission in the 15 days before: members 61 to 160). The rest of the members are set equal to the deterministic control.

The LETKF uses the covariance matrix of the observations and that of the prior to estimate the background covariance matrix **B** in the observational space, and to propagate the increments from the ensemble space to the control vector. Our modified ensemble is not strictly in line with the needed assumptions, as it artificially includes members without perturbed emissions. To counteract this issue, we have introduced an inflation factor equal to the number total members (100) over the number of perturbed members (20), that is multiplied with the LETKF **Y** matrix (i.e., the covariance matrix of the ensemble in the observational space). In the observation space this value of inflation might underestimate the contribution of perturbations from previous days (in AOD). On the other hand, each chunk of 3-days perturbation is initialised from the deterministic runs, meaning that the emission perturbations are gradually accounted for in the AOD field during the model time integration, which would mean that the inflation value might be overestimated. Actually, these two terms approximately cancel each other, meaning that the missing influence of the same-day emission perturbation is compensated by emissions perturbations of previous days, and thus the inflation of 20/100 seems to be an appropriate guess.

We further fine-tuned the inflation by computing the Desroziers diagnostic on innovations. In this ensemble, the $\mathbf{HBH^T}$ matrix is simply the covariance matrix of the ensemble AOD collocated with the observations. Figure 6 shows bi-dimensional histograms of the square root of the ratio between the trace of the $\mathbf{HBH^T}+\mathbf{R}$ matrix and the trace of the $\mathbf{d^o_b}\,(\mathbf{d^o_b})^T$ matrix, with $\mathbf{d^o_b}$ the departures of the prior (observation minus background) AOD. Figure 6 shows this ratio binned by the value of the assimilated observation (VIIRS on the top row) and using AERONET in the bottom row. While we use the estimate of **R** for VIIRS to compute this diagnostic, we set the observational error for AERONET close to zero. Under these conditions of very small **R**, the comparison of the trace of both matrices ($\mathbf{HBH^T}$ and $\mathbf{d^o_b}\,(\mathbf{d^o_b})^T$) is equivalent to the commonly used ratio between the ensemble spread to the root mean square error of the forecast (Fortin et al., 2014). For most common AOD values in the VIIRS panel, where the density of points in the histograms is maximum, a ratio of ~1.58 is found. Therefore, under the assumption that the estimate of **R** is correct, we adopt an optimal inflation of 1.58^2 = 2.5 over the ensemble variance, that would provide a better error balance in the system, according to this diagnostic on innovations.

	Using IFS-COMPO DOD (x1.5)	Using IFS-COMPO AOD
VIIRS	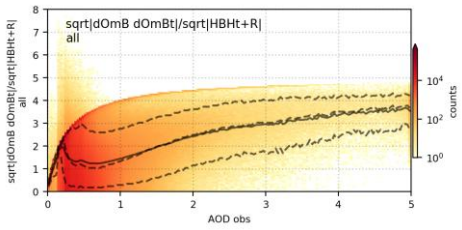	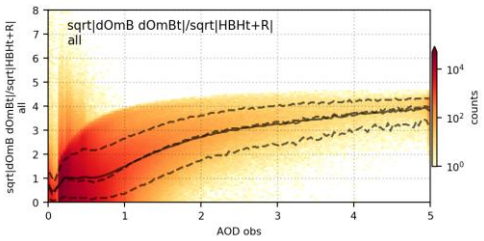
AERONET (ang<0.3, all stations)	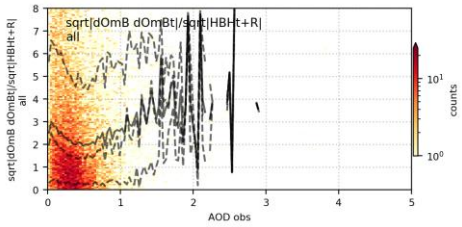	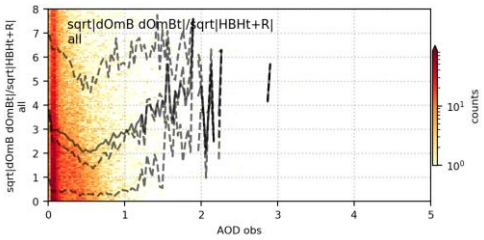

Figure 6: Histograms of innovation diagnostics in the observation space. Values are presented as functions of the observed AOD (x-axis), and the ratio between the square root of the trace of the $\mathbf{d^o_b}$ $(\mathbf{d^o_b})^T$ matrix and the square root of the trace of the $\mathbf{HBH^T+R}$ matrix (y-axis). Upper row shows the diagnostic for the VIIRS dust-filtered AOD (with prescribed error of 0.2xAOD + 0.05) and the lower row shows the diagnostics for Ångström-filtered AERONET AOD (with negligible prescribed error). Results from a dust AOD assimilation experiment (DUODx1.5_SCALING) is shown on the left and from a total AOD assimilation experiment (AOD_SCALING) on the right. For qualitative assessment, averaged values are shown in continuous lines and 10, 50 and 90 percentiles in segmented lines.

3.6 Assimilation experiments

We have produced, with the same ensemble, two sets of emission correction factors. Preliminary comparison of the deterministic first guess runs shows that the simulated dust AOD is systematically lower than the assimilated VIIRS dust-filtered AOD (Fig. 4, top panels). This is expected, since the dust-filtered AOD from VIIRS is, by definition, total AOD and not only dust. Following the analysis of Figure 4, we estimated a bias correction factor 1.5 that is applied to the dust AOD would compare better with VIIRS dust-filtered AOD. A second experiment was produced by using total AOD in the observation operator. In both cases, we apply an inflation of the background covariance matrix equal 2.5.

4 Results: emissions scaling factors

4.1 Emission scaling factors

Figures 7 and 8 show seasonal estimates of dust emissions for the two sets of scaling factors, using 1.5xDOD (denoted as the DUODx1.5_SCALING experiment) in Figure 7 and AOD (denoted as the AOD_SCALING experiment) in Figure 8. Both figures show the prior average daily emissions, the average analysis emissions, the ratio between them and the difference between them.

In general, both experiments agree on the spatial and seasonal corrections, while some relatively small variations are apparent between seasons. In the increments (xa-xb) and averaged correction factors (xa/xb), it can be noted the length scale of the perturbations used

to produce the ensemble. As stated before, this is the effective spatial resolution that the system can resolve, thus, it is an expected behaviour. In addition, although there is a large seasonal variation on global dust emissions (from ~2780 Tg/yr –yearly equivalent– in boreal spring, to ~6000 Tg/yr –yearly equivalent– in boreal autumn), the assimilation produces global changes of less than 10% of the prior emissions.

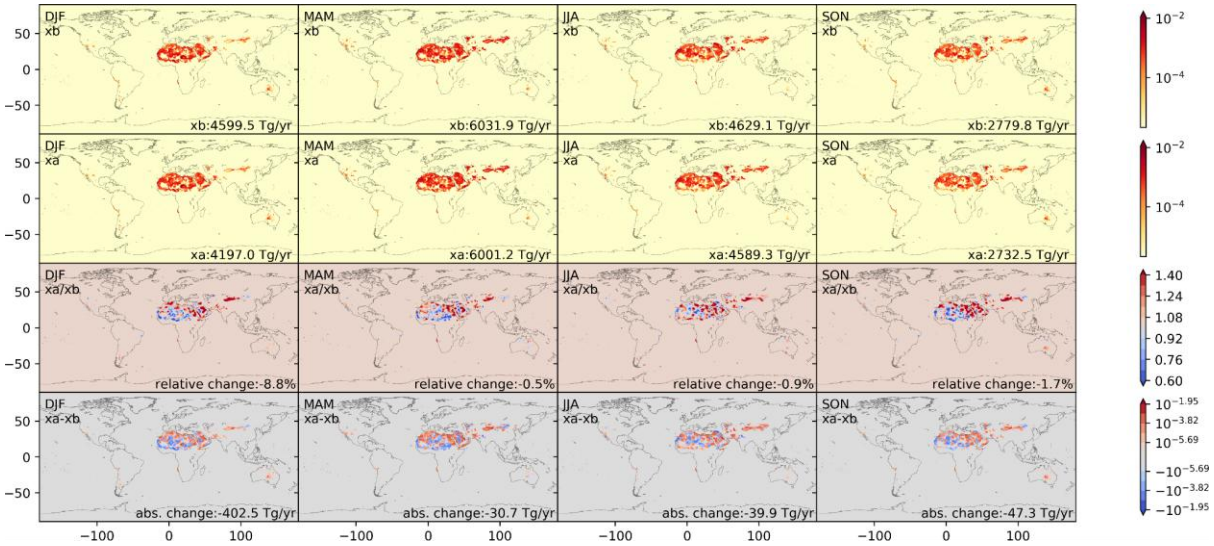

Figure 7: Seasonal emissions for the DUODx1.5_SCALING experiment. Rows: average prior daily emissions (kg m^{-2} day^{-1}), average analysis emissions (kg m^{-2} day^{-1}), ratio of the average analysis to prior emissions, average increments (kg m^{-2} day^{-1}).

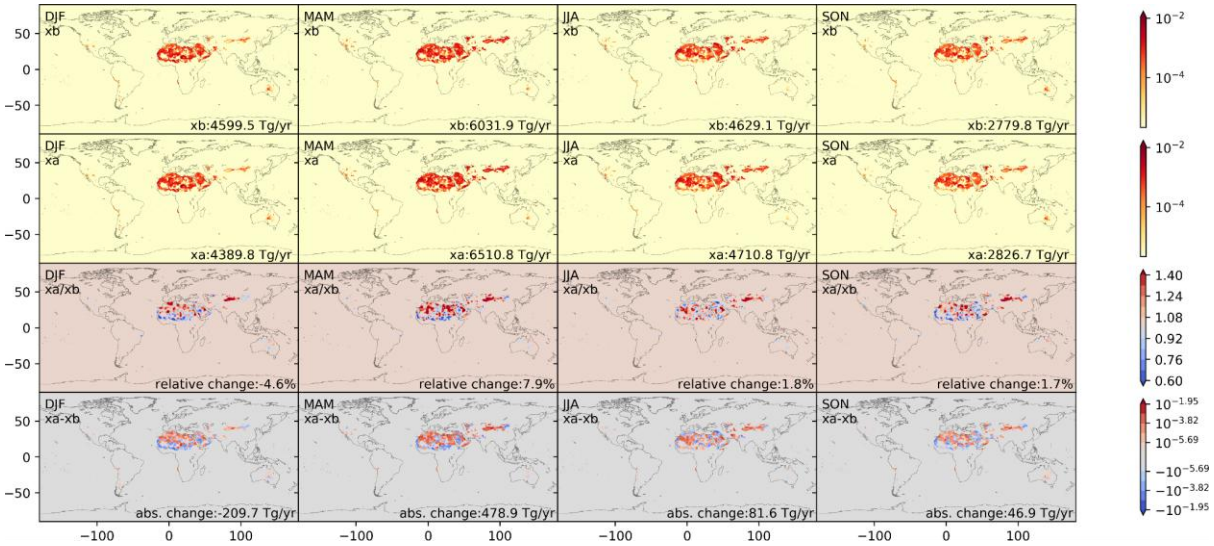

Figure 8: Seasonal emissions for the AOD_SCALING experiment. Rows: average prior emissions (kg m^{-2} day^{-1}), average analysis emissions (kg m^{-2} day^{-1}), ratio of the average analysis to prior emissions, average increments (kg m^{-2} day^{-1}). Please note the logarithmic colour scale in rows 1, 2 and 4.

The temporal averaging of Figures 7 and 8 might mask the temporal variations of the actual emission increments at the source scale. Figure 9 shows the time series on four selected sites, computed by daily 2017-2022 multi-year averages. For periods when the emissions are non-negligible, the correction factors obtained from the data assimilation (left), can show values

between 0.5 to 2, depending on the site and time of the year. The right panel shows the impact of these correction factors on the emissions. In some cases, like the point in Mauritania (second row), the correction is systematic around June. This figure also shows the impact of the inflation of **B** by comparing the red and blue lines. In a general way, when comparing the two assimilation cases, with and without inflation, the adoption of a 2.5 inflation factor ("i2.5") only increases the departures of the correction factors from to the line of 1 (i.e., the line without corrections) with respect to the no-inflation case ("i1"). In any case, please note this difference between the no-inflation case and i2.5 does not always correspond to an *a-posteriori* linear inflation of the increment.

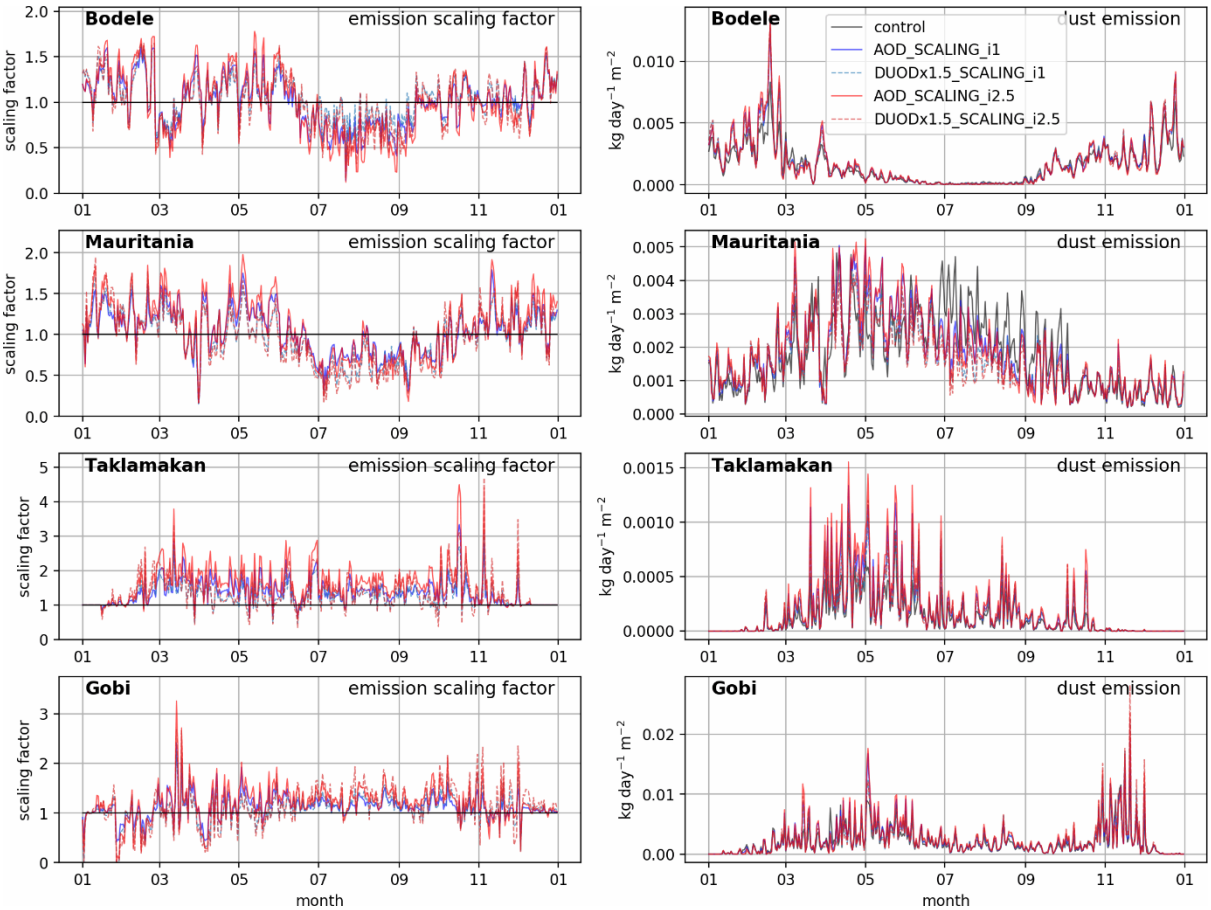

Figure 9: Yearly cycle (average of the 5 years) of the prior and analysis correction factor (left) and dust emission (right, in Kg m^{-2} day^{-1}) for four selected sites: Bodélé (17N, 17.75E), Mauritania (26N,12W), Taklamakan (19N,82E) and Gobi (42N,100E). Gray line shows the prior, blue lines show the results of the assimilation without inflation ("i1") in the ensemble and red lines show the assimilation with ensemble inflation ("i2.5"). Continuous lines show the experiments of DUODx1.5_SCALING, dashed lines the experiments with AOD_SCALING. Please note that the x-axis should be read as a generic year.

4.2 Use in forecast only IFS-COMPO simulations

A series of IFS-COMPO forecast-only simulations have been set up in order to assess the impact of the use of the dust emissions scaling factor on the skill of simulated fields. The years 2017 and 2019 have been processed with three experiments each (see Table 1 for details of the experiments).

Forecast-only simulations mean that no data assimilation of aerosol related fields is carried out: the aerosol and chemistry initial conditions of each cycle is taken from the 24h simulation

from the previous cycle, while the meteorological initial conditions are taken from an operational simulation which uses data assimilation. Experiments have been designed to apply the scaling factor from the two datasets (DUODx1.5_SCALING and AOD_SCALING) to dust emissions at the same date, and to test the use of a monthly mean of the AOD_SCALING scaling factor, called AODMONTH_SCALING.

Table 1: Summary of the IFS-COMPO experiments with the analyses emission scaling factors.

experiment name	experiment id	specifics
REF	ijjq (2017) / ifdp (2019)	Reference experiment
AOD_SCALING	iot6(2017) / iot7(2019)	Experiment using daily dust emissions scaling factor derived using simulated total AOD (see section 3.6 for more details).
DUODx1.5_SCALING	iot8 (2017) / iot9 (2019)	Experiment using daily dust emissions scaling factor derived using simulated dust AOD x 1.5 (see section 3.6 for more details).
AODMONTH_SCALING	ioum (2017) / ioun (2019)	Experiment using monthly (as averaged over 2017-2021) dust emissions scaling factor derived using simulated dust AOD x1.5.

The objective of the AOD_SCALING and DUODx1.5_SCALING experiment is to assess whether the use of the emissions scaling factor improve the skill scores of simulated AOD by IFS-COMPO against observations not used in the offline inversion process: AERONET AOD. The AODMONTH_SCALING investigates whether the use of mean scaling factors could improve the skill of the simulated AOD. Given the strong daily variations of the scaling factors (see Figure 9), this is not a guaranteed.

We first compare the simulated mean dust emissions (which include the effect of the scaling factors) of the three experiments in Figure 10, for two months in 2017. In both January and May 2017, there are common features between AOD_SCALING and DUODx1.5_SCALING, notably the low scaling factors in January over most of the Sahel, indicating a systematic high bias of the operational dust emission scheme in the area. Another common feature, in May 2017, are the high scaling factors over the Taklimakan and Gobi area, and an area of lower scaling factors over inner Mongolia. On the other hand, areas with strong disagreements between the two experiments also exist, such as most of the Arabic peninsula (low scaling factor with AOD_SCALING and high with DUODx1.5_SCALING). Over the Sahara, the patterns look quite different between the two experiments in January, but quite similar in May.

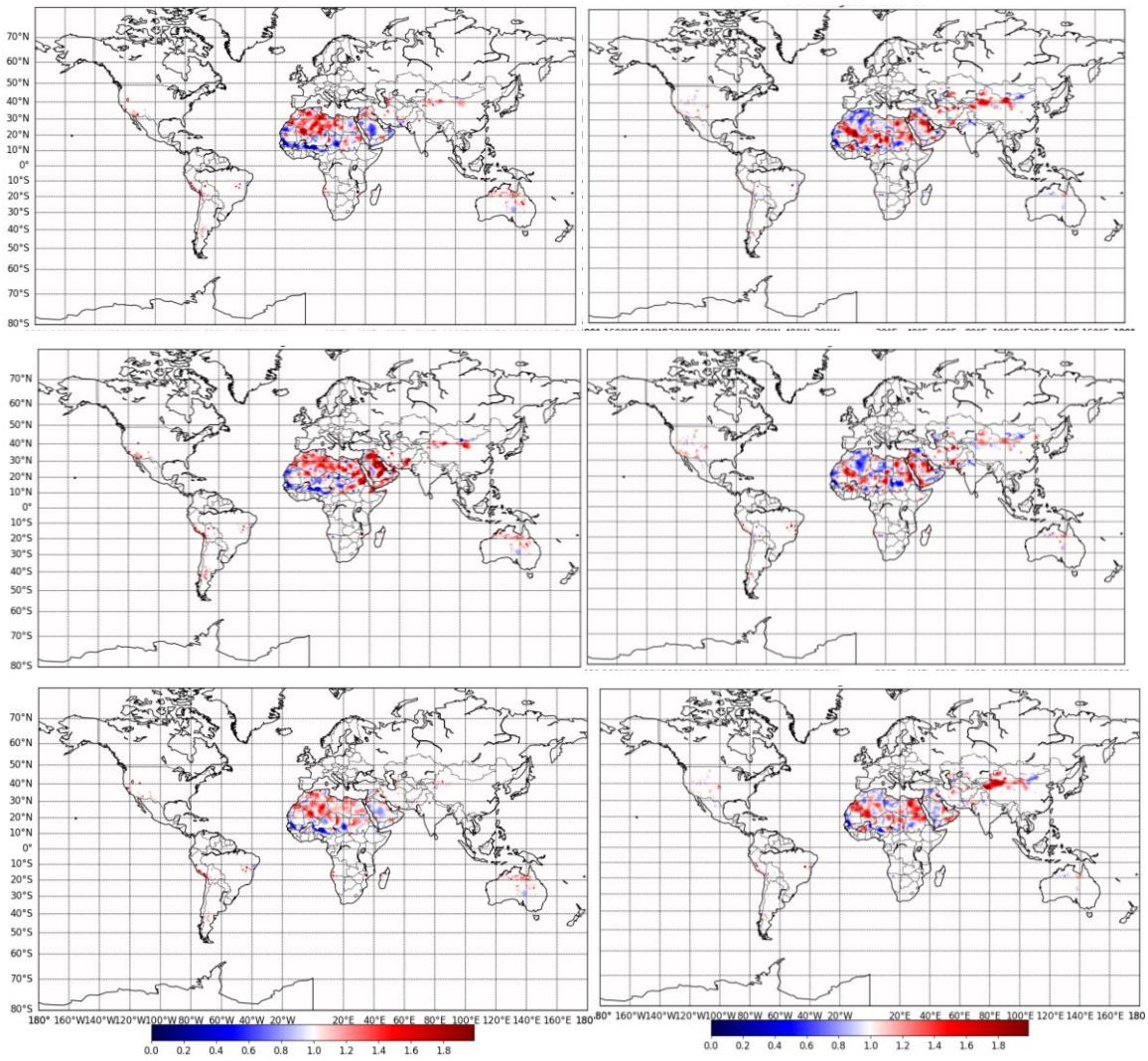

Figure 10: Ratio of mean monthly AOD_SCALING (top), DUODx1.5_SCALING (middle) and AODMONTH_SCALING (bottom) over REF dust emissions in January (left) and May (right); 2017. Red means that the scaled emissions emissions are higher than those of REF.

We then focus on AOD_SCALING in Figure 11 for different years. The 2017 and 2019 values are shown to assess how the yearly variability of dust events impacts the scaled dust emissions. January and May are shown to show how the scaling factors are season dependent. There are similarities and differences between the 2017 and 2019 ratio between scaled and reference dust emissions. In January, dust emissions are mostly increased over Western Sahara and significantly decreased over most of Sahel areas. The patterns are similar between 2017 and 2019, but the values differ slightly. Over Eastern Sahara and the Arabian Peninsula, there are more differences between 2017 and 2019. Dust emissions over the Taklimakan desert are always increased by AOD_SCALING, more so in May than in January. In May, dust emissions are mostly increased over Eastern Sahara, while Western Sahara show some areas with consistent and inconsistent scaling between 2017 and 2019. The Arabian Peninsula shows mostly increased dust emissions in May 2017 with AOD_SCALING and mostly decreased in May 2019

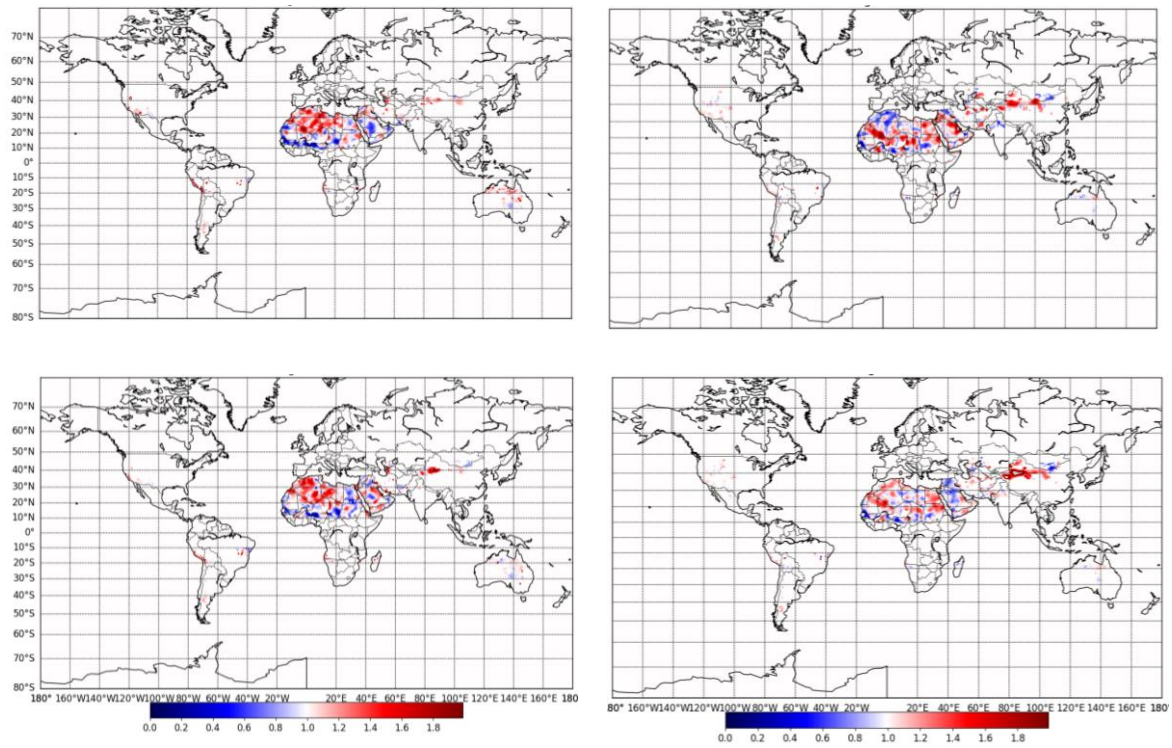

Figure 11: Ratio of mean monthly AOD_SCALING over REF dust emissions in January (left) and May (right); 2017 (top) and 2019 (bottom). Red means that AOD_SCALING emissions are higher than those of REF.

The 2017 simulations are evaluated first in terms of impact on simulated dust AOD at 550nm, as shown in Figure 12. The simulated dust AOD at 550nm by REF shows the usual higher values close to the main source regions: the Western Sahara, Arabic Peninsula, Taklimakan and Gobi deserts. The simulated AOD by AOD_SCALING shows the strongest differences over the Taklimakan desert, with an increase in simulated DOD of around 20%. The simulated DOD is also higher over parts of Eastern and Western Sahara, by up to 10%. On the other hand, the simulated DOD is strongly reduced, by up to 30%, over the Southern fringes of the Sahara. The DUODx1.5_SCALING experiment shows mostly lower DOD values over most of the Sahara, except over the same parts of Eastern Sahara that saw higher DOD with AOD_SCALING. The Taklimakan area also shows slightly higher simulated DOD with DUODx1.5_SCALING. Finally, AODMONTH_SCALING shows lower simulated DOD values almost everywhere.

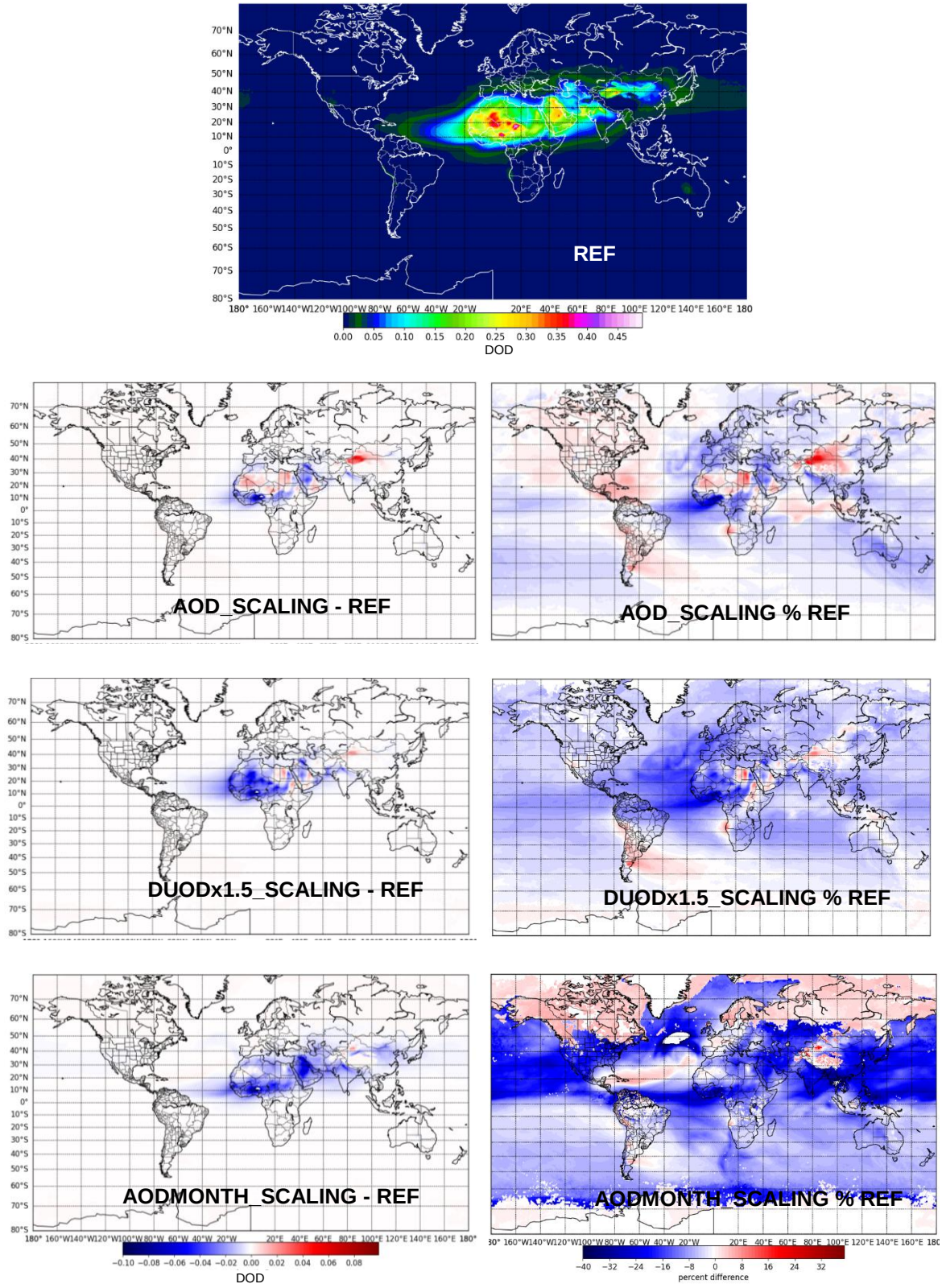

Figure 12: 2017 DOD at 550nm simulated by REF (single top panel); differences in absolute DOD values (left) and relative differences in percentages of the REF DOD (right) for AOD_SCALING (second row), DUODx1.5_SCALING (third row) and AODMONTH_SCALING (fourth row) experiments.

An evaluation of simulated AOD at 500 and 1020nm has been carried out against AERONET observations over a selection of stations usually impacted by desert dust (Figure 13). The impact of the use of the scaling factors is relatively small, and no clear positive signal is evident on the RMSE of the simulated AOD. The same conclusion can be reached when a filter on Ångström exponent is applied to select only situations dominated by desert dust (not shown). This rather small impact could be caused by three factors:

- The signal on AOD is weaker than that on dust AOD because a significant fraction of aerosols is simulated to be from other species, even over most of desertic AERONET sites;
- The relative impact of the scaling factors of the dust emissions is limited by the fact that they concern relatively small areas, arising from the choice of correlation length of 250km. A higher correlation length could increase the ensemble spread and lead to scaling factors that have a larger geographical footprint;
- Temporal averaging (of one week) and spatial averaging (over the globe) of the AERONET and simulated AOD can mask the differences between simulations.

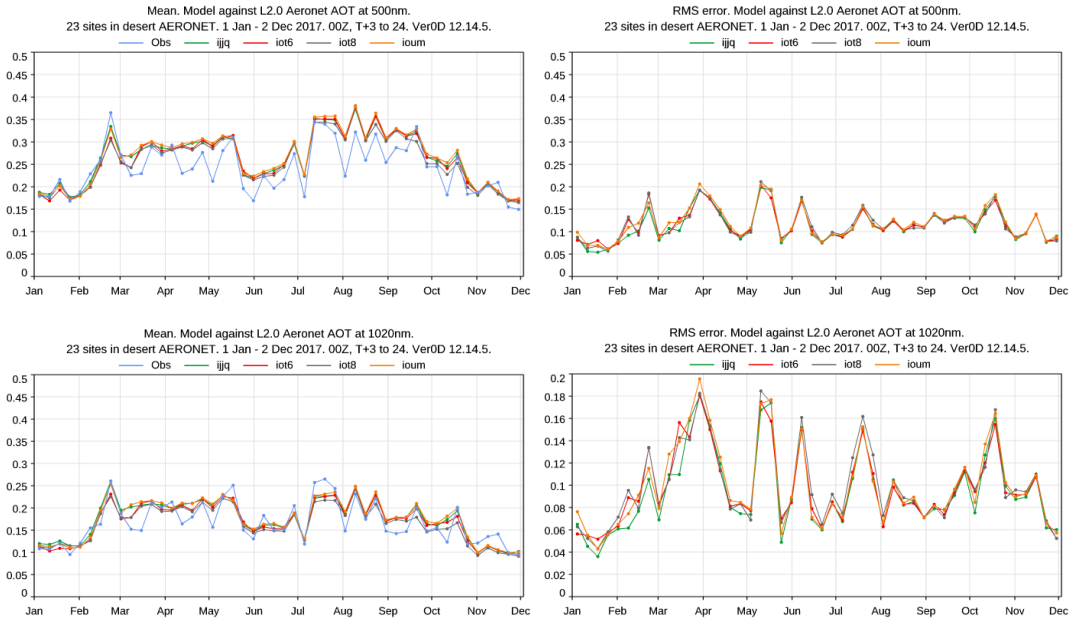

Figure 13: 2017 weekly observed and simulated AOD at 500nm (top left) and 1020nm (bottom left). Right, RMSE of weekly simulated AOD at 500nm (top right) and 1020nm (bottom right). Evaluation done on a selection of 23 AERONET stations representative of desert dust. The experiments shown are REF (**green**), AOD_SCALING (**red**), DUODx1.5_SCALING (**gray**) and AODMONTH_SCALING (**orange**).

This conclusion can be refined by examining density scatterplots of daily observed versus simulated AOD at 500nm over the same selection of dust impacted AERONET stations (Figure 14). Only situations in which the observed Ångström exponent is less than 0.3 are presented, so the plots correspond to situations when desert dust was observed. We can see that the use of the daily dust emissions scaling factors (AOD_SCALING and DUODx1.5_SCALING) lead to a small but noticeable increase in the correlation coefficient between observed and simulated values, while the use of monthly scaling factors actually leads to a degradation of the same correlation. This indicates a small but positive impact of the use of the daily dust emissions scaling factor. Nonetheless, the impact is much smaller than hoped for, which is why a new ensemble simulation has been started, as described in Section 5.

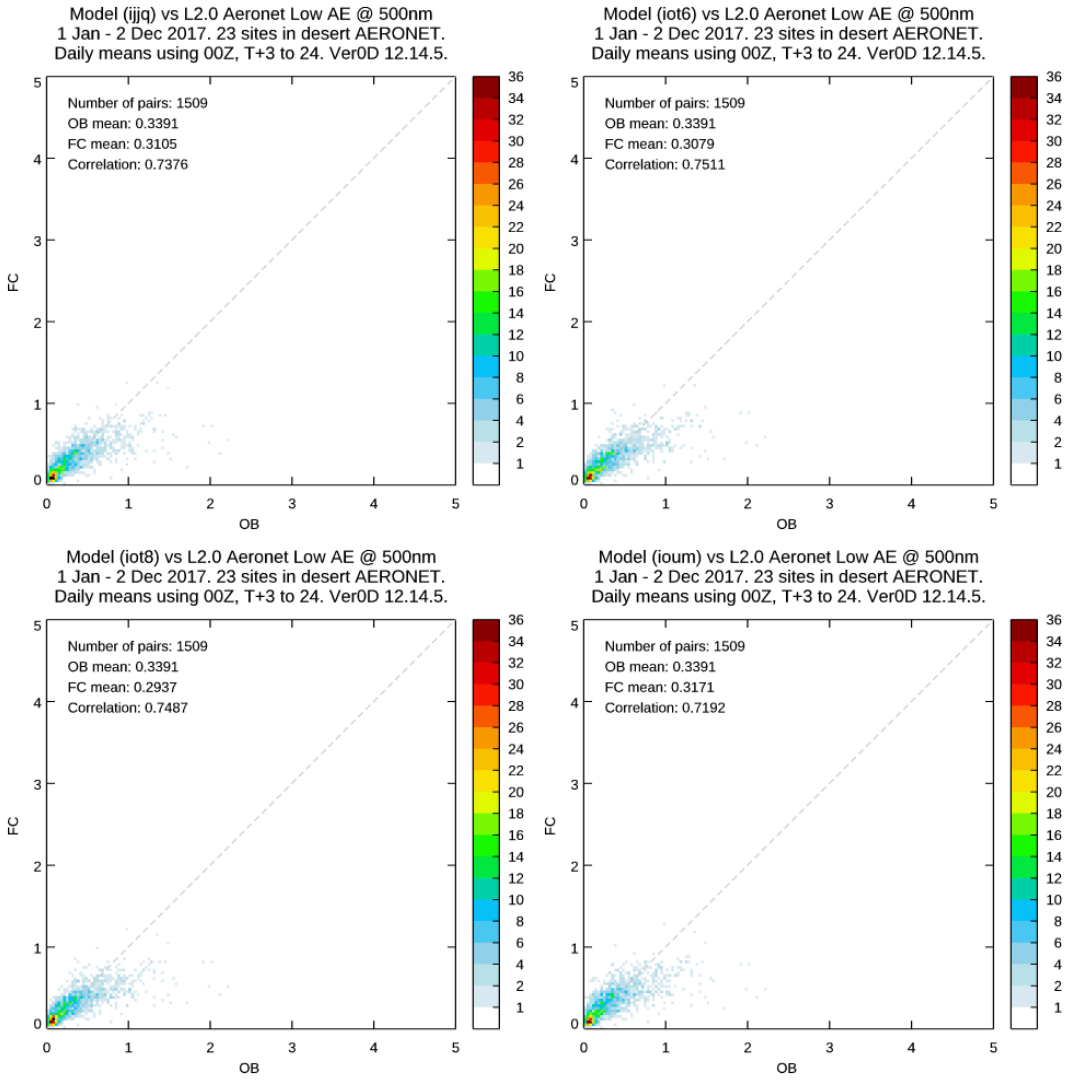

Figure 14: Density scatterplots of simulated (y-axis) versus observed (x-axis) AOD at 500nm over a selection of stations more impacted by desert dust, and only for situations where the observed Ångström exponent is below 0.3 (dusty situation).

The aggregated scores versus AERONET hide some stronger impact when looking at individual stations (Figure 15). Tamanrasset is located at the heart of the Sahara, while Dakar and Ilorin are at its Western and Southern fringes respectively. The impact of the scaling factors is significant, but no strong improvement is visible.

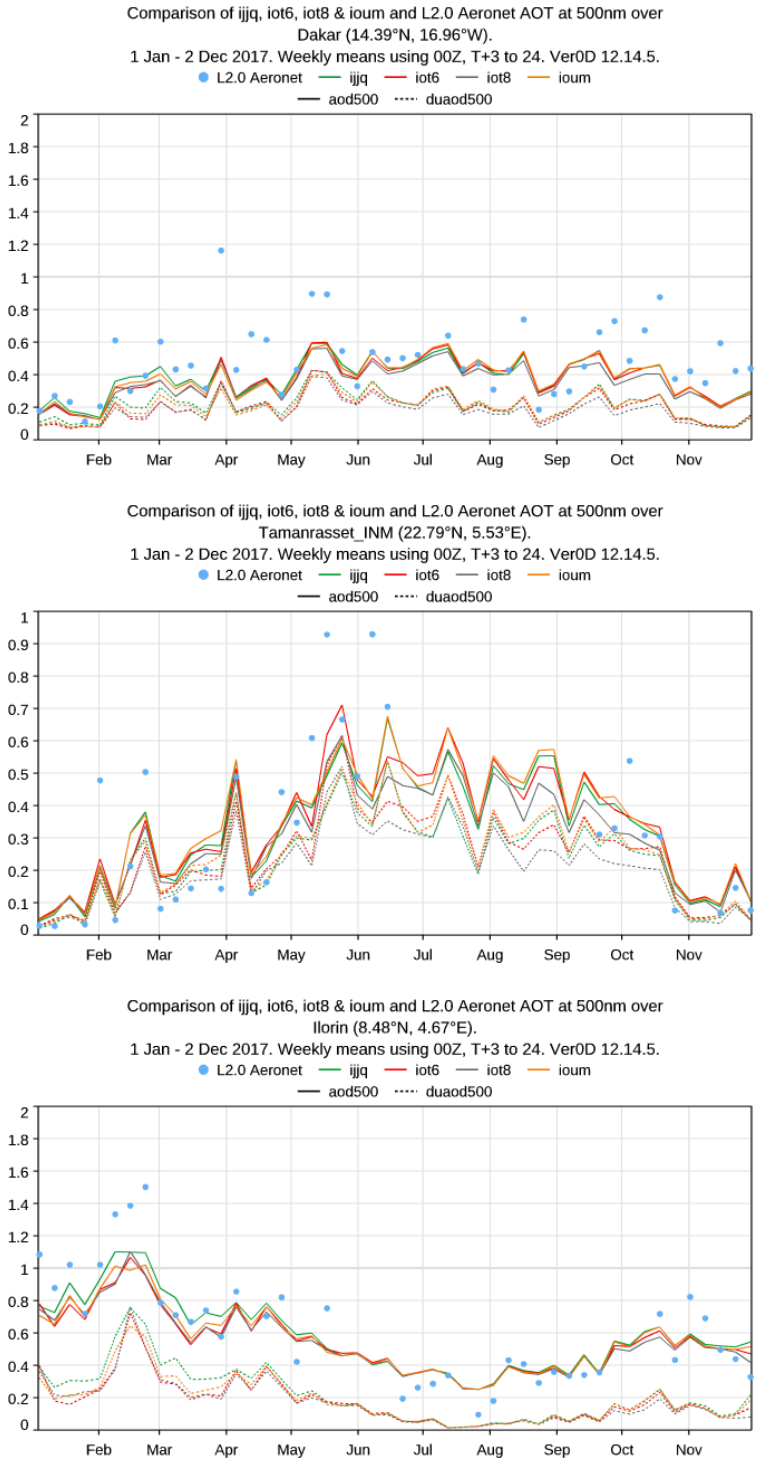

Figure 15: 2017 weekly observed and simulated AOD (solid lines) and DOD (dashed lines) at 500 nm over Dakar (top), Tamanrasset (middle) and Ilorin (bottom). The experiments shown are REF (**green**), AOD_SCALING (**red**), DUODx1.5_SCALING (**gray**) and AODMONTH_SCALING (**orange**). AERONET observations are shown in blue dots.

Finally, we examine the impact of the dust emission scaling factor during a series of large dust storms over most of China in April and May 2017, in terms of simulated AOD and PM10 (Figure 16). REF shows a significant overestimation in simulated PM10 during the mid-April 2017 event, with values above 200 μg/m^3 against around 100 μg/m^3 observed. Conversely, a significant underestimation is noted for the early May 2017 event, which witnessed observed

PM10 averaged over all background rural stations in China close to 300 µg/m^3, with values above 150 µg/m^3 simulated by REF. AOD_SCALING, and to a lesser extent DUODx1.5_SCALING, bring a decrease in simulated AOD and PM10 in mid-April, and a small increase in simulated PM10 in early May, thus increasing the skill of the forecasts for this particular situation. This may be caused by the fact that the dust storm of mid-April originated over inner Mongolia, with less than 1 scaling factors from AOD_SCALING and DUAODx1.5_SCALING, while the early May dust event originated from Gobi/Taklimakan, where the scaling factors are higher than 1.

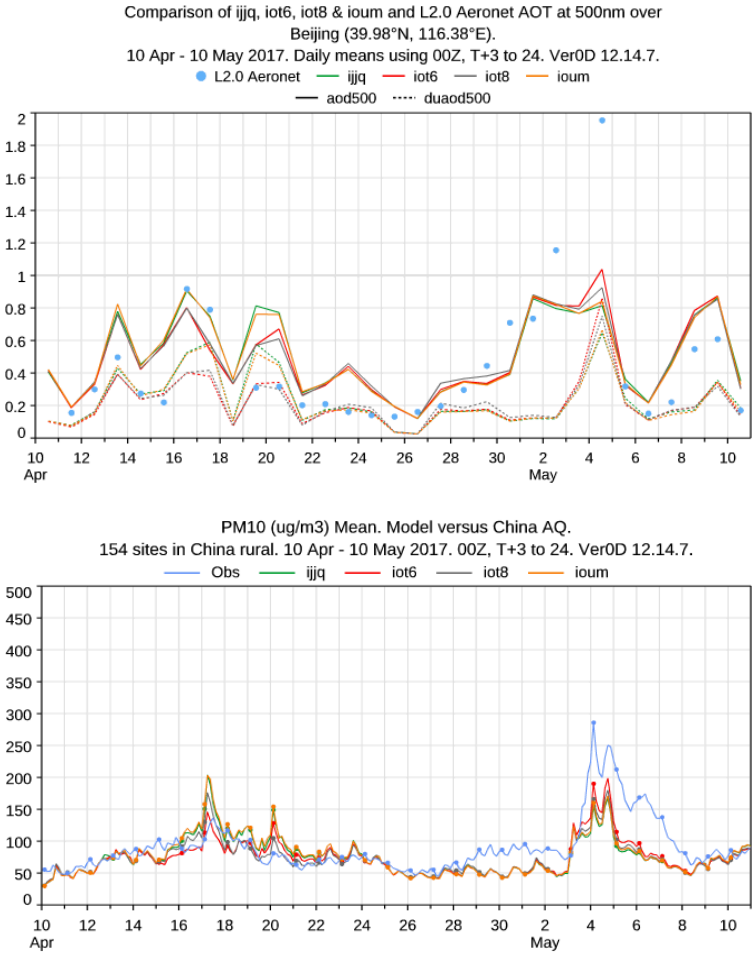

Figure 16: April and early May 2017, daily observed and simulated AOD at 500nm over Beijing (top) and PM10 over background rural stations in China (bottom). The experiments shown are REF (**green**), AOD_SCALING (**red**), DUODx1.5_SCALING (**gray**) and AODMONTH_SCALING (**orange**).

5 Use of new dust emission scheme and varying correlation lengths

Following the results shown in Section 4, a new IFS-COMPO dust ensemble has been set up, which uses varying correlation lengths, as well as the new dust emission scheme developed in Work Package 5. For a description of the dust emission scheme, please refer to deliverable 5.1.

Figure 17 shows the perturbation map used in this new ensemble. It contains 20 maps with correlation length (L) between 300 km to 3000 km, equally distributed in log(L). One year of

IFS-COMPO has been produced. With these simulations, we have produced preliminary correction factors, which are shown in Figure 18 and Figure 19; but we have not yet produced the analyses AOD.

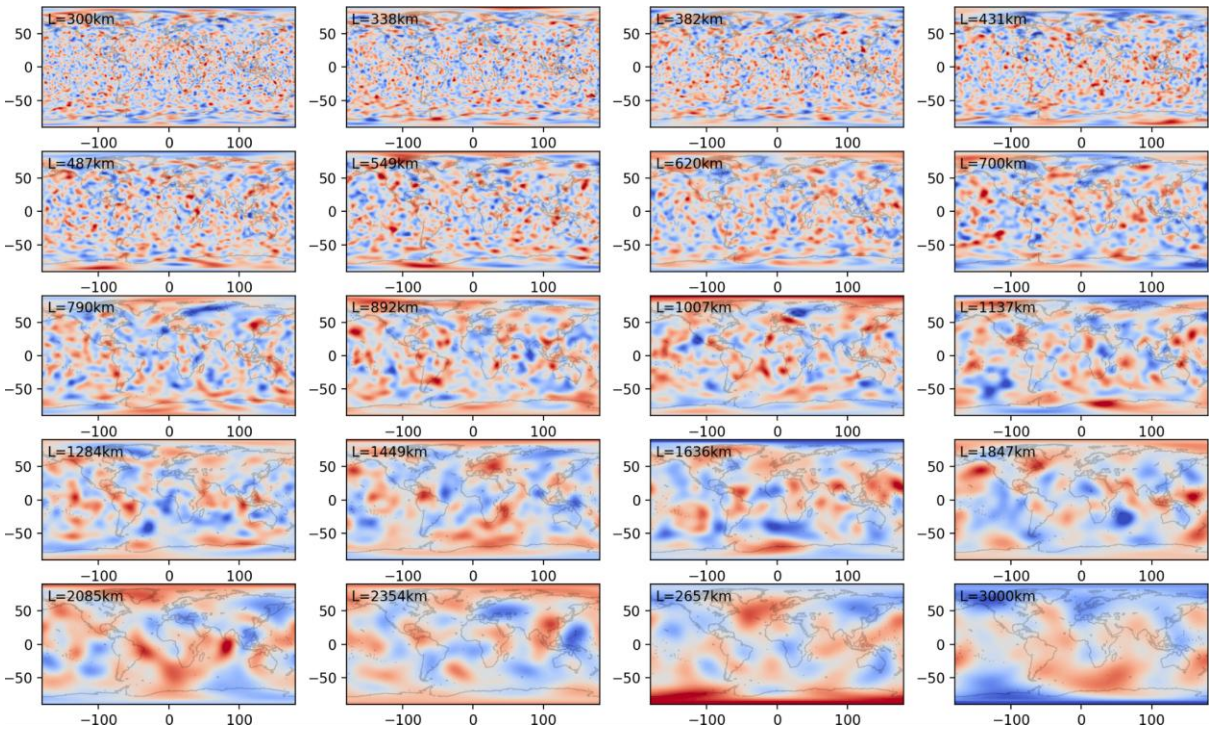

Figure 17: Random gaussian perturbation maps with length scale ranging from 300 km to 3000 km used in the new ensemble generation.

Both experiments with the new ensemble from Figures 18 and 19 show smoother spatial corrections, in concordance with the larger correlation length of the perturbations. There are clear seasonal changes in the corrections over Central and East Sahara, and China's deserts. Globally averaged emission increments at the seasonal scale are considerably larger than those of the first ensemble.

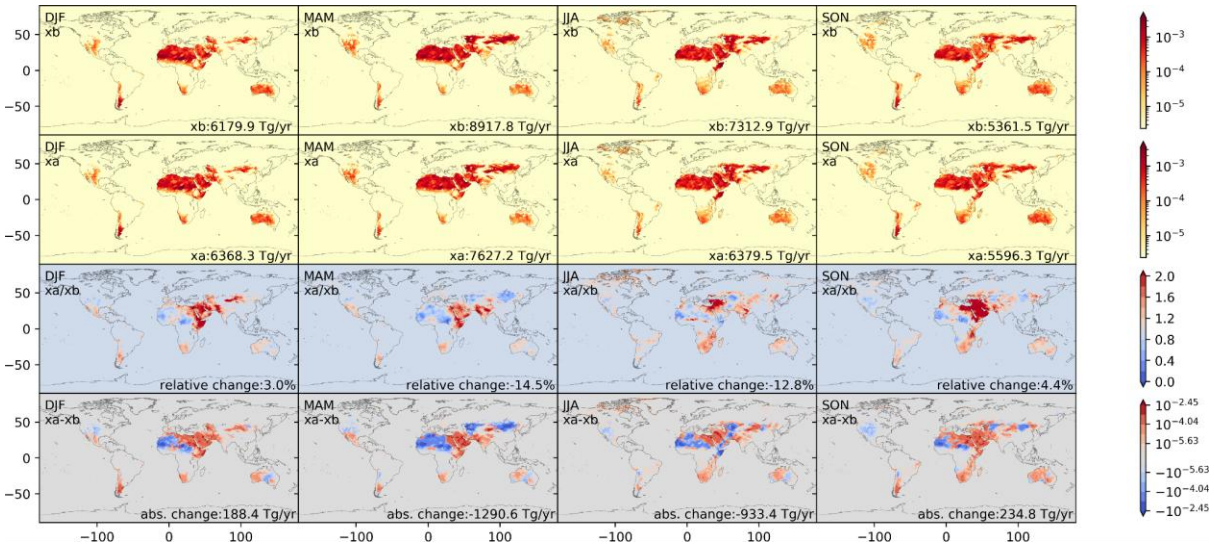

Figure 18: Same as Figure 7 (DUODx1.5_SCALING) but for the new ensemble. Preliminary results only for 2017.

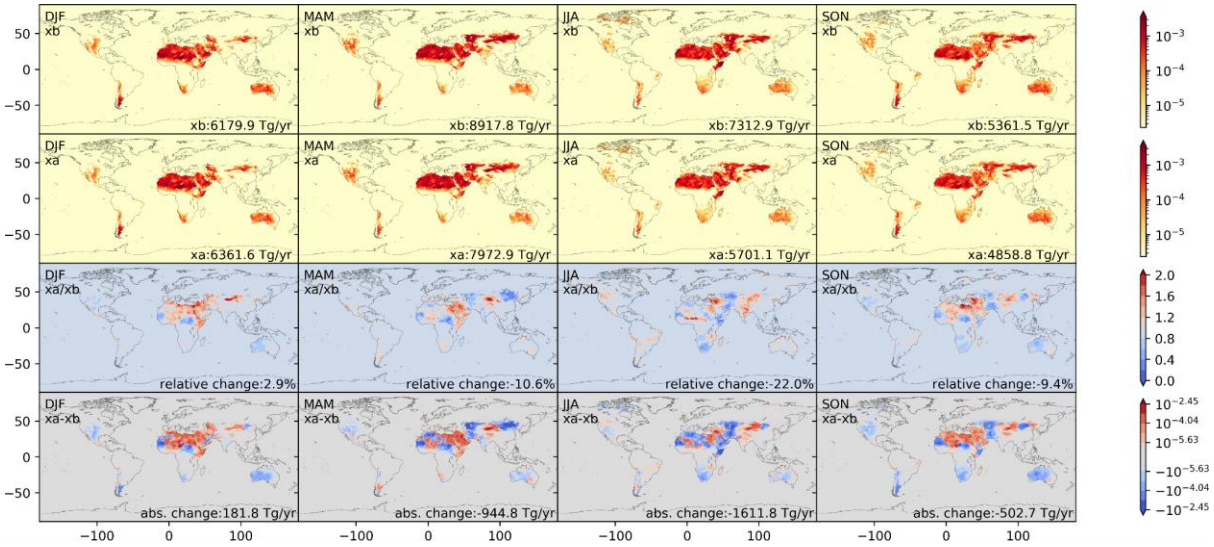

Figure 19: Same as Figure 8 (AOD_SCALING) but for the new ensemble. Preliminary results only for 2017.

Yearly averaged emissions and corrections for the first and the second ensembles are shown in Figure 20. We showcase only the AOD assimilation experiment, and for the second ensemble we show only preliminary results for the year 2017.

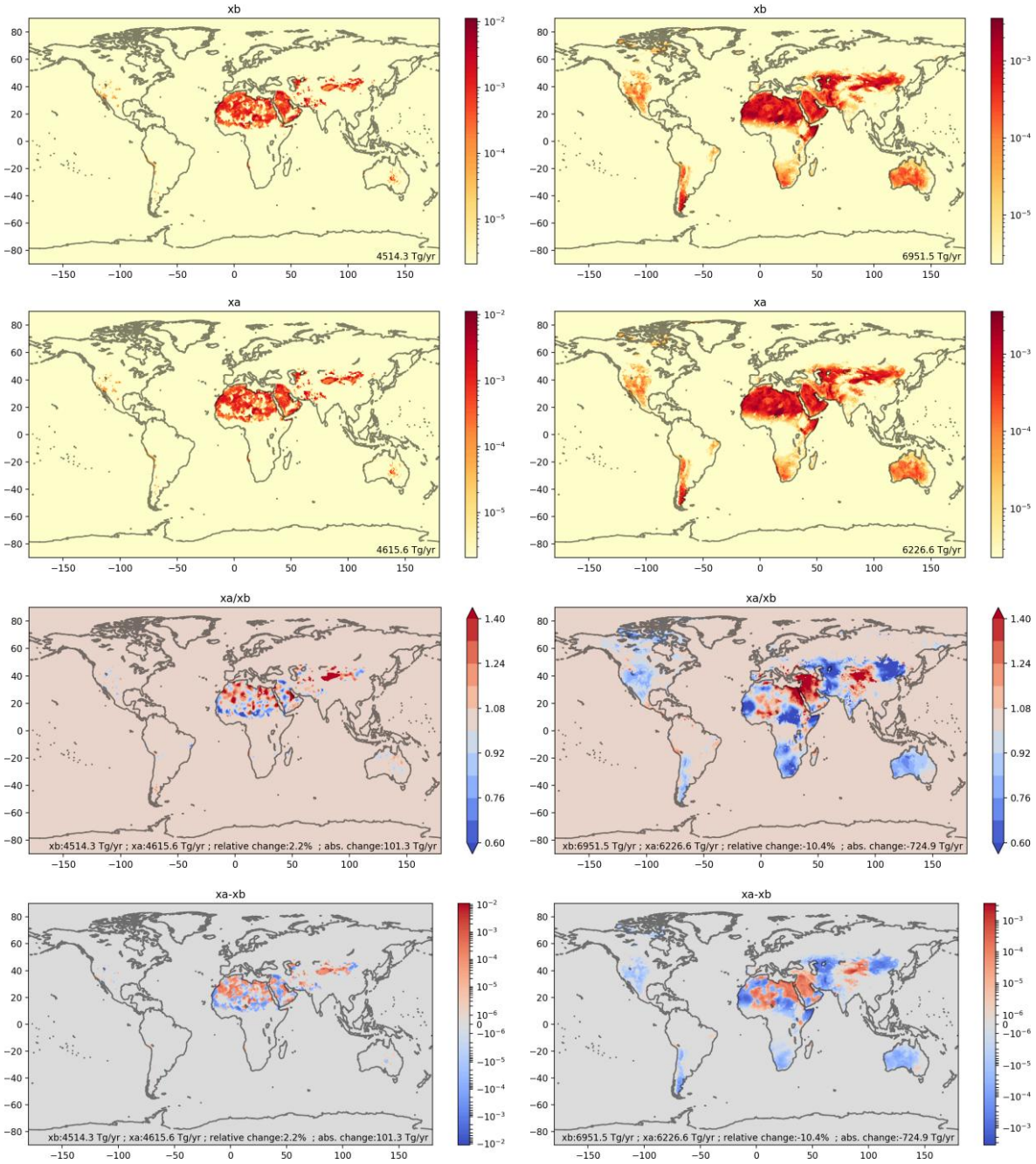

Figure 20: From top to bottom: averaged prior daily emissions (kg m^{-2} day^{-1}), analysed emissions (kg m^{-2} day^{-1}), ratio of analysis to prior emissions, and emission increments. The first ensemble is shown in the left panel and the new ensemble on the right. Both columns show the AOD assimilation experiment. Please note the different colour scales.

There is a notable difference in the spatial distribution of the prior emissions, as well as in their total amount of emissions. While the first ensemble produces around 4500 Tg/yr, the second emits 6950 Tg/yr over larger regions. The assimilation has more impact on the second ensemble, yielding a 10% decrease on the total emissions (only 2.2% for the first ensemble).

6 Conclusion

In this document we have implemented an offline dust emission inversion system for IFS-COMPO. The ability of the inversion to attribute analysis increments to the appropriate emission time is embedded in the setup of the ensemble and the assimilation method is adjusted accordingly. A five-years ensemble of IFS-COMPO simulations has been produced, and two data assimilation experiments were performed. Before assimilation, the Dust AOD ensemble was unbiased. We have adjusted the background covariance matrix inflation according to innovation diagnostics for both experiments.

The control run shows good skills when compared to ground-based AOD over a selection of AERONET sites. Ensemble emission and atmospheric load show an expected seasonal cycle with spread in concordance with the perturbations spatial scale and strength.

A posteriori emissions show consistent increments in space and season, and also between experiments in most of the emission regions. However, the global amount of emission changes due to the assimilation in these experiments is very low (around 2% of the mass flux). A third forecast experiment was created by producing monthly averages of the AOD correction factors, with very similar results.

Spatial averages of the simulated AOD show maximum increments of around ±10% of the prior AOD, while in absolute terms the average increments are still small (order of 0.02 of AOD). The comparison with ground-based weekly averages of AERONET AOD show very small improvements when they are globally averaged, and second-digit improvements in the correlation coefficient for daily values. When time series of AERONET sites are not averaged, the positive impact of the assimilation on the evaluation scores is larger. The offline dust inversion is also useful in pointing areas with systematic biases, such as the too high dust emissions over most of the Sahel, and the too low emissions over the Taklimakan/Gobi area.

In addition to these results, we show the latest development on the ensemble generation, with preliminary results of the emission estimation. For this purpose, we also used the dust scheme developed in D5.1. All in all, various caveats in the first ensemble seem to be mitigated, and preliminary results are promising.

7 Bibliography

Adebiyi, A. A., Kok, J. F., Wang, Y., Ito, A., Ridley, D. A., Nabat, P., and Zhao, C. (2020). Dust Constraints from joint Observational-Modelling-experiMental analysis (DustCOMM): comparison with measurements and model simulations, Atmos. Chem. Phys., 20, 829–863, https://doi.org/10.5194/acp-20-829-2020.

Escribano, J.; Boucher, O.; Chevallier, F.; Huneeus, N. (2016). Subregional inversion of North African dust sources. Journal of Geophysical Research: Atmospheres. 121-14, pp.8549-8566. ISSN 2169-8996., https://doi.org/10.1002/2016JD025020

Escribano, J.; Boucher, O.; Chevallier, F.; Huneeus, N. (2017). Impact of the choice of the satellite aerosol optical depth product in a sub-regional dust emission inversion. Atmospheric Chemistry and Physics. 17-11, pp.7111-7126. https://doi.org/10.5194/acp-17-7111-2017

Escribano, J., Di Tomaso, E., Jorba, O., Klose, M., Gonçalves Ageitos, M., Macchia, F., Amiridis, V., Baars, H., Marinou, E., Proestakis, E., Urbanneck, C., Althausen, D., Bühl, J., Mamouri, R.-E., and Pérez García-Pando, C. (2022). Assimilating spaceborne lidar dust extinction can improve dust forecasts, Atmos. Chem. Phys., 22, 535–560, https://doi.org/10.5194/acp-22-535-2022

Fortin, V., Abaza, M., Anctil, F., & Turcotte, R.. (2014). Why Should Ensemble Spread Match the RMSE of the Ensemble Mean?. Journal of Hydrometeorology, 15(4), 1708-1713. https://doi.org/10.1175/JHM-D-14-0008.1

Hunt, B., Kostelich, E., Szunyogh.,I (2007). Efficient data assimilation for spatiotemporal chaos: A local ensemble transform Kalman filter. Physica D: Nonlinear Phenomena, Volume 230, Issues 1–2, 112-126, https://doi.org/10.1016/j.physd.2006.11.008.

A1. Selected AERONET sites

List of the 23 AERONET sites dominated by dust used in this report: Tizi_Ouzou, Tamanrasset_INM, SEDE_BOKER, Mezaira, Masdar_Institute, Lampedusa, KAUST_Campus, Izana, Tunis_Carthage, Ilorin, Santa_Cruz_Tenerife, La_Laguna, Dakar, Dalanzadgad, Cairo_EMA, Dushanbe, Arica, Gobabeb, Windpoort, Ben_Salem, Capo_Verde, La_Parguera, Teide, and El_Farafra. Figure A1 shows the location of these 23 sites.

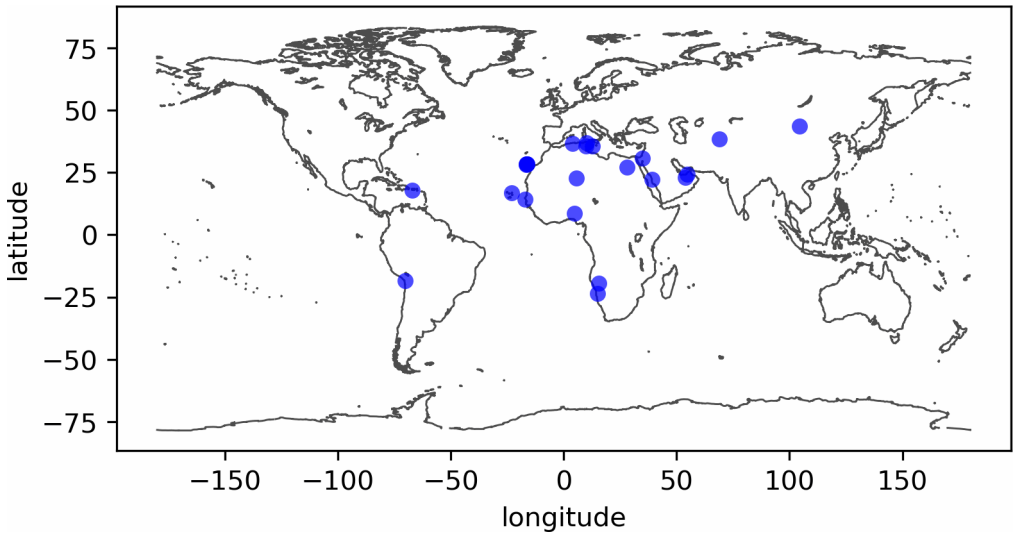

Figure A1: Location of the 23 AERONET sites.

A2. Table of Acronyms

AERONET	Aerosol Robotic Network
AOD	Aerosol optical depth
AOD_SCALING	Assimilation experiment using AOD from IFS-COMPO
AODMONTH_SCALING	Assimilation experiment using AOD from IFS-COMPO but with monthly scaling factors
BSC	Barcelona Supercomputing Center
CAMAERA	CAMS Aerosol Advancement
CAMS	Copernicus Atmosphere Monitoring Service
DA	Data assimilation
DOD	Dust aerosol optical depth
DUODx1.5_SCALING	Assimilation experiment using 1.5 x DOD from IFS-COMPO
ECMWF	European Centre for Medium-Range Weather Forecasts
HPC	High Performance Computing
I/O	Input/Output
IFS	Integrated forecasting System
IFS-COMPO	Atmospheric composition configuration of IFS
LETKF	Local Ensemble Transform Kalman Filter
REF	Control IFS-COMPO simulation
RMSE	Root Mean Squared Error
SUOMI-NPP	Suomi National Polar-orbiting Partnership
VIIRS	Visible Infrared Imaging Radiometer Suite
WP	Work Package

Document History

Version	Author(s)	Date	Changes
1.0	J.Escribano and S.Remy	11-06-2025	Initial version
1.1	J. Escribano	25-06-2025	Including A1, A2, Comments for SMHI and MET Norway addressed

Internal Review History

Internal Reviewers	Date	Comments
Ana Carvalho (SMHI)	16-06-2025	Keep acronyms harmonized, and include a table with those could be helpful. Please see other comments in the text.
Arjo Seger (MET Norway)	19-06-2025	Minor corrections